

Provided for non-commercial research and education use.  
Not for reproduction, distribution or commercial use.



This article appeared in a journal published by Elsevier. The attached copy is furnished to the author for internal non-commercial research and education use, including for instruction at the authors institution and sharing with colleagues.

Other uses, including reproduction and distribution, or selling or licensing copies, or posting to personal, institutional or third party websites are prohibited.

In most cases authors are permitted to post their version of the article (e.g. in Word or Tex form) to their personal website or institutional repository. Authors requiring further information regarding Elsevier's archiving and manuscript policies are encouraged to visit:

<http://www.elsevier.com/copyright>



## Simulation of ultrashort double-pulse laser ablation

Mikhail E. Povarnitsyn<sup>a,\*</sup>, Tatiana E. Itina<sup>a,b</sup>, Pavel R. Levashov<sup>a</sup>, Konstatntin V. Khishchenko<sup>a</sup>

<sup>a</sup> Joint Institute for High Temperatures RAS, Izhorskaya 13 Bldg 2, Moscow 125412, Russia

<sup>b</sup> Laboratoire Hubert Curien, UMR CNRS 5516, 18 rue Benoît Lauras, Bât. F, 42000 St-Etienne, France

### ARTICLE INFO

#### Article history:

Available online 2 December 2010

#### Keywords:

Double-pulse ablation  
Crater formation  
Suppression of ablation

### ABSTRACT

In this paper, we study the mechanisms of femtosecond double-pulse laser ablation of metals. It was previously shown experimentally that the crater depth monotonically drops when the delay between two successive pulses increases. For delays longer than the time of electron–ion relaxation the crater depth can be even smaller than that produced by a single pulse. The results of the performed hydrodynamic simulation show that the ablation can be suppressed due to the formation of the second shock wave. The modeling results of the double-pulse ablation obtained for different delays correlate with the experimental findings.

© 2010 Elsevier B.V. All rights reserved.

### 1. Introduction

An application of the double-pulse (DP) technique in laser-induced breakdown spectroscopy [1] can give higher luminosity of plasma in comparison with a single pulse (SP) of the same entire energy and thus improve the accuracy of measurements. Performing femtosecond DP irradiation of different metals several authors [2–4] surprisingly noticed a monotonic decrease in the ablation crater depth with increasing delay  $\tau_{\text{delay}}$  between pulses. This effect was observed both in the presence of ambient air [2] and in vacuum [3,4]. In the experiment [4] with copper targets the laser fluence of each pulse was set to be  $F_{\text{single}} = 2 \text{ J/cm}^2$ , the pulse width 100 fs and the laser wavelength 800 nm. The ablation crater depth as a function of the delay is shown in Fig. 1.

For delays much shorter than the electron–ion relaxation time in material ( $\tau_{\text{ei}} = 10 \text{ ps}$  for copper [5]) the crater depth was the same as in the case of a SP with the laser fluence  $2F_{\text{single}} = 4 \text{ J/cm}^2$ . For the delays close to the electron–ion relaxation time ( $\tau_{\text{delay}} \sim \tau_{\text{ei}}$ ), the crater depth monotonically decreased. Similar dynamics of crater formation was also obtained for other metals (aluminum [2], gold [4] and nickel [3]). The authors of Refs. [2,3] also claimed that at  $\tau_{\text{delay}} > \tau_{\text{ei}}$  the DP crater depth could be smaller than that obtained using a SP with the same fluence as for each pulse in the DP. The first results on the simulation of DP ablation have been published recently [6]. In this article we continue to investigate the interplay of physical mechanisms in DP ablation and highlight the analysis of compression, tensile waves and phase states in copper at different delays between pulses.

### 2. Model

A hydrodynamic model [7,8] was developed and previously used for simulation of a SP laser ablation of metals. The model contains the multiphase wide-range equation of state (EOS) in tabular form allowing an accurate treatment of metastable phases and phase transitions [9]. The specific Helmholtz free energy has a form  $F(\rho, T_i, T_e) = F_i(\rho, T_i) + F_e(\rho, T_e)$ , composed of two parts which describe the contribution of heavy particles and electrons, respectively. Here,  $\rho$  is the material density and  $T_i$  and  $T_e$  are the temperatures of heavy particles and electrons. The first item,  $F_i(\rho, T_i) = F_c(\rho) + F_a(\rho, T_i)$ , in turn, consists of the electron–ion interaction term  $F_c$  (calculated at  $T_i = T_e = 0 \text{ K}$ ) and the contribution of thermal motion of heavy particles  $F_a$ . The solid, liquid, and gas phase equilibrium boundaries are determined from the equality conditions for the temperature  $T_i$ , pressure  $P_i = \rho^2(\partial F_i / \partial \rho)_{T_i}$ , and Gibbs potential  $G_i = F_i + P_i / \rho$  of each phase pair. The free energy of electrons in metal  $F_e$  has a finite-temperature ideal Fermi-gas form [10].

In Fig. 2 the phase diagram of copper with stable and metastable phases is shown. The metastable phases are indicated by the corresponding first letters in square brackets, the stable ones—without brackets. In simulation the metastable phases of overheated liquid [l] and overcooled gas [g] are taken into account. Currently we do not consider overheated solid and overcooled liquid; while the last is not significant for fast heating processes, the first can play a noticeable role for femtosecond laser pulses with smaller fluences. In the future we plan to investigate the influence of the solid phase overheating on the ablation in metals.

A possibility of the existence of negative pressures in condensed matter should be considered in fast and ultra-fast processes. In fact, the target matter is always metastable under such conditions. The used multiphase equation of state can work with three metastable

\* Corresponding author.

E-mail address: [povar@ihed.ras.ru](mailto:povar@ihed.ras.ru) (M.E. Povarnitsyn).

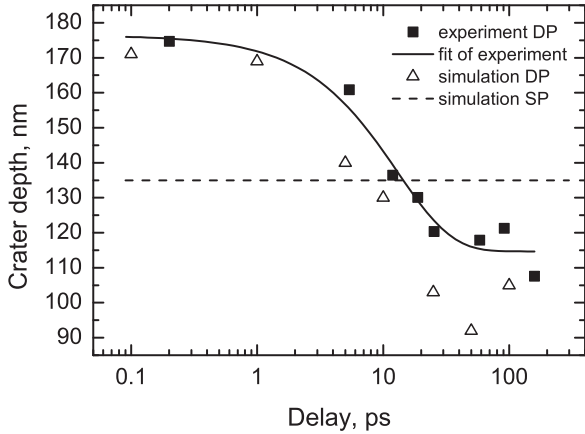


**Fig. 1.** Crater depth as a function of the delay between the pulses. (■) Experiment [4], (△) simulation (this work), solid line—fit of experiment [4], and dash line—crater depth in SP simulation (this work).

phases at negative pressures: metastable solid [s], metastable melting [s+l] and metastable liquid [l]. The boundary between the metastable state of liquid at positive and negative pressures can be estimated by the position of the isobar  $P=0$  GPa in Fig. 2. The regions of metastable liquid and metastable melting are artificially restricted from below at some temperature (and the region of metastable solid from the left at some density) to simplify the calculation of thermodynamic functions at negative pressure; these restrictions have no influence on the results.

The multiphase equation of state returns the information about the phase state and phase and metastable states boundaries; this fact allows us to switch to the kinetics and fragmentation mechanisms depending on the phase state of matter.

In the simulations of SP experiments, the approximation of laser energy absorption by a simple Lambert–Beer’s law is satisfactory; using this approach we obtained good agreement with SP experimental findings for several metals [9]. In DP ablation experiments, however, this simplified technique fails for the second pulse because of surface smearing and inhomogeneity of target properties produced by the first pulse. To overcome this problem the Helmholtz wave equation for the electric component of the laser

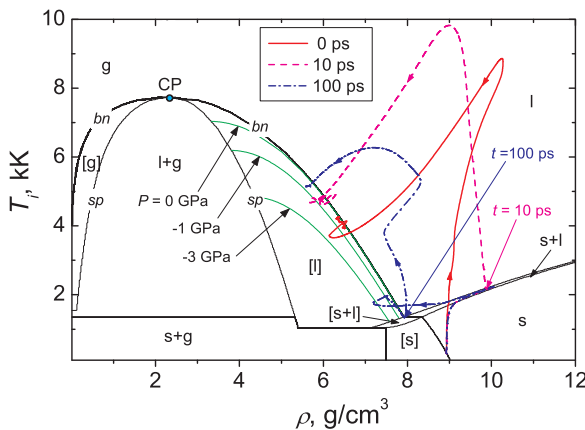


**Fig. 2.** Phase diagram of copper. CP: critical point; bn: the binodal; sp: the spinodal; g: stable gas; l: stable liquid; s: stable solid; s+l: stable melting; l+g: liquid–gas mixture; s+g: solid–gas mixture; [g]: metastable gas; [l]: metastable liquid; [s+l]: metastable melting; [s]: metastable solid. Solid (green) lines— isobars  $P=0$ ,  $-1$ , and  $-3$  GPa. Solid (red) line—phase trajectory of the target layer with initial coordinate  $z=60$  nm for  $\tau_{\text{delay}}=0$ , dash (magenta) line—for  $\tau_{\text{delay}}=10$  ps, and dash-dot line—for  $\tau_{\text{delay}}=100$  ps. (For interpretation of the references to color in this figure legend, the reader is referred to the web version of the article.)

pulse with normal incidence [11] is used:

$$\frac{\partial^2 E}{\partial z^2} + k_0^2 \epsilon(\omega_L, \rho, T_e, T_i) E = 0 \quad (1)$$

in the region  $z_1 \leq z \leq z_2$  for the first and second pulses. Here  $E(z, t)$  is the  $x$ -component of the slowly varying in time laser field amplitude,  $E_x(z, t) = E(z, t) \exp(-i\omega_L t)$ ,  $k_0 = \omega_L/c$  is the laser wave vector with the laser frequency  $\omega_L$  and the light speed in vacuum  $c$ . The boundary conditions for  $\partial E/\partial z$  at  $z=z_1$  and  $z=z_2$  are lengthy and can be found elsewhere [11].

A wide-range model of complex permittivity of matter was used in the form  $\epsilon = (1/2)(\epsilon_{\text{met}} + \epsilon_{\text{pl}}) - (1/2)(\epsilon_{\text{met}} - \epsilon_{\text{pl}}) \tanh(2T_e/T_F - 2)$ , where  $T_F$  is the Fermi temperature. This approximation describes the Drude-like limit  $\epsilon_{\text{met}}(\omega_L, \rho, T_e, T_i)$  in solid state (for copper  $\epsilon_{\text{met}} = -27.6 + 2.7i$  at normal conditions and 800 nm wavelength [12]) and the plasma limit  $\epsilon_{\text{pl}}(\omega_L, \rho, T_e)$  in hot ionized gas state [13]. In metals for chosen parameters of laser wavelength and intensity the inverse Bremsstrahlung mechanism of absorption is dominant and thus the heat source can be expressed as  $Q_{\text{IB}} = I_0 k_0 \text{Im}\{\epsilon\} |E/E_0|^2$ ,  $I_0$  is the peak laser intensity,  $E$  is the solution to the Helmholtz equation and  $E_0 = \sqrt{8\pi I_0}/c$  is the maximum of laser electric field in vacuum.

For realistic treatment of the fragmentation process, the model based upon the homogeneous nucleation mechanism [9] is used. Three basic stages are assumed to take place in the fragmentation model: (i) spontaneous appearance of critical size gas bubbles, (ii) growth of these bubbles, and (iii) confluence of bubbles and final relaxation of pressure and temperature. All these stages are present in the code. Simulations of the DP ablation show that pressure in copper can be as low as  $P_{\text{min}} = -3.6$  GPa [6]. Such pressure values were shown to result in the mechanical spallation in the liquid phase. In the solid phase, however, the spallation strength for high strain rates ( $\rho^{-1} \partial \rho/\partial t \sim 10^{10} \text{ s}^{-1}$ ) is close to its theoretical limit (the pressure on the cold curve at the same density) which is substantially lower than  $P_{\text{min}}$ . For example, at  $\rho = 8 \text{ g/cm}^3$  the multiphase EOS gives  $\approx -10$  GPa at  $T_i = 0$ .

The experiment [4] for copper target was reproduced numerically applying two Gaussian laser pulses with normal incidence, 100 fs width, 800 nm wavelength and fluence  $2 \text{ J/cm}^2$  each. The peak intensity of the first and second pulses corresponds to moments  $t = 0$  ps and  $t = \tau_{\text{delay}}$ , respectively, and initial surface position is at 0 nm.

### 3. Results and discussion

To illustrate the process of the DP ablation we choose a  $z = 60$  nm depth layer of the copper target at initial time  $t = -0.5$  ps. Then the evolution of thermodynamic and kinematic parameters of this layer during the simulation with  $\tau_{\text{delay}} = 0, 10$  and 100 ps is analyzed. In Fig. 2 the phase trajectories of the referred above layer by solid (0 ps), dash (10 ps) and dash-dot (100 ps) lines are shown.

All the trajectories originate in one and the same point at normal conditions for copper. The trajectory with  $\tau_{\text{delay}} = 0$  (solid line in Fig. 2) is equivalent to the SP ablation with the doubled fluence  $4 \text{ J/cm}^2$ . It crosses the melting region almost along the normal isochore and then evolves into the liquid phase where it reaches supercritical temperatures because of the fast heating of electrons by the laser pulse and energy transfer from electrons to ions during  $t \sim \tau_{\text{ei}}$ . The heating of ions gives rise to the formation of the shock wave (SW) spreading into the target; the compression of matter is also visible along the  $\tau_{\text{delay}} = 0$  trajectory. Then the tensile wave (TW) arrives at layer under consideration, and the matter begins to expand. The trajectory enters into the metastable liquid region at negative pressures where the mechanical fragmentation process begins; this leads to the fluctuations of thermodynamic parameters along the trajectory.

For the trajectory with  $\tau_{\text{delay}} = 10$  ps (dash line in Fig. 2) the fluence of the first pulse is  $2\text{ J/cm}^2$ , therefore the heating and compression of the considered layer is lower than in the case of  $\tau_{\text{delay}} = 0$  ps. At  $t = 10$  ps (see the arrow in Fig. 2) the second laser pulse gives rise to the sharp increase in temperature; for the dielectric permittivity model used we obtain even higher temperatures than those in the case of  $\tau_{\text{delay}} = 0$  ps. Then again the trajectory comes into the metastable liquid region at negative pressures because of the TW propagation.

Finally, the trajectory with  $\tau_{\text{delay}} = 100$  ps (dash-dot line in Fig. 2) shows the most peculiar behavior. During the first 10 ps it obviously coincides with the trajectory with  $\tau_{\text{delay}} = 10$  ps, but then the TW comes into play, and the density and temperature along the trajectory diminish up to the metastable liquid region at negative pressure. One can see that pressure on the trajectory drops below  $-3$  GPa, and then the fragmentation process gives rise to the relaxation of pressure up to 0 GPa. At this moment (100 ps, shown by the arrow in Fig. 2) the second pulse arrives, thus establishing the rise of temperature and density variation. The last can be explained by the complex non-uniform distribution of density and temperature in the fragmented material in which the second pulse is absorbed. Nevertheless, the density higher than at  $t = 100$  ps is reached before the second TW provides for the drop of temperature and density and causes the trajectory to enter into the metastable liquid phase again where fragmentation of the target material continues. It should be noted however, that the second TW is weaker than the first one, that is why the ablation process and fragmentation is less pronounced in this case.

The previous calculations [8,9] have demonstrated that only the melted region can be ablated due to the TW propagation. Further, if the second pulse arrives when the TW goes through the liquid layer, this second pulse reheats the nascent ablation plume. As a result, a high-pressure region is generated in the vicinity of the initial target surface. In this reheated region the SW forms and moves into the bulk suppressing the action of the first TW. Therefore, the depth of the crater drops. We are going to discuss this effect in detail using the time-space diagrams (Figs. 3 and 4).

For  $\tau_{\text{delay}} = 0$  ps the formation of melting front (s+l cyan region) is seen. The thickness of the melted region reaches about 180 nm by the time delay of 40 ps after the first pulse maximum. After the heating of ions, the SW arises with the maximal pressure behind the front  $\sim 35$  GPa (Fig. 3b). At the same time the high-pressure heat-affected zone begins to expand in two rarefaction waves; one appears on the free surface of the target and moves into the bulk, the other moves from the end of the heat affected zone towards the free surface. As a result of the rarefaction waves interaction a zone of negative pressure arises and the minimal pressure trace in this TW is schematically shown in Fig. 3a and b. Mechanical fragmentation starts after the propagation of the TW and by the moment 60 ps the voids in liquid layer have been formed. The speed of the fastest liquid layer on the interface between liquid (yellow) and liquid-gas mixture (orange) is about 500 m/s. The boundary between the high-density (metastable liquid) and low-density (liquid-gas mixture) phases is denoted by b1 in both Fig. 3a and b; it has a negative slope and moves away from the target; the same can be observed for the region of metastable melting [s+l] (magenta in Fig. 3a). The liquid-gas mixture and gas (red for the metastable phase and dark blue for the stable) fractions form the front of the nascent ablation plume.

For 100 ps delay one can clearly see in Fig. 4b that two SWs (SW1 and SW2) are formed; the pressure behind the first SW is approximately 3 times higher than that behind the second one. These two SWs are separated by the TW, the path of which (TW1) is also shown in Fig. 4a and b.

The second pulse produces an extension of substance (dash line TW2 in Fig. 4a and b), but this effect is weak and does not con-

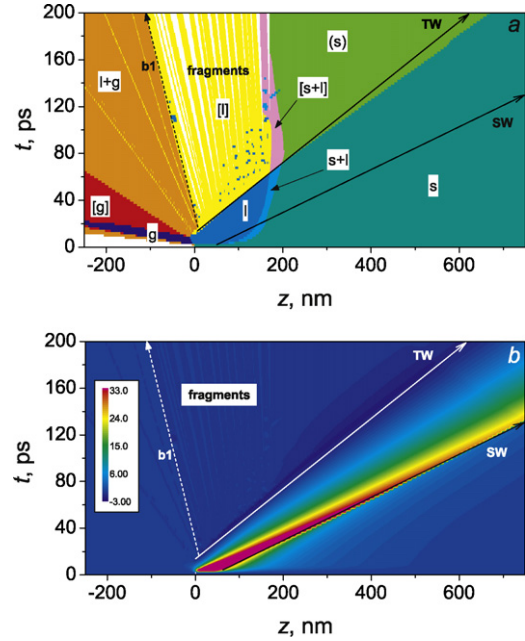


Fig. 3.  $z$ - $t$  diagrams of phase states (a) and pressure in GPa (b) in the target for  $\tau_{\text{delay}} = 0$ . Presented phase states are: s: solid (olive); s+l: melting (light blue); l: liquid (blue); l+g: liquid-gas mixture (orange); g: gas (dark blue); [s]: metastable solid (green); [l+g]: metastable melting (magenta); [l]: metastable liquid (yellow); [g]: metastable gas (red). For interpretation of the references to color in this figure legend, the reader is referred to the web version of the article.)

tribute much in fragmentation of matter; the pressure behind the second SW (SW2) drops more slowly than behind the first one (SW1). The boundary between high-density and low density phases is also shown in Fig. 4a and b by b1–b3. It is remarkable that after the first TW the boundary b1 has a negative slope, then after the second SW b2 has a positive slope and after the second TW b3 is almost vertical, or, in other words, its velocity is nearly zero. It means that the second pulse produces an increase in the atomization of the ablation plume head and compression and recoil of the

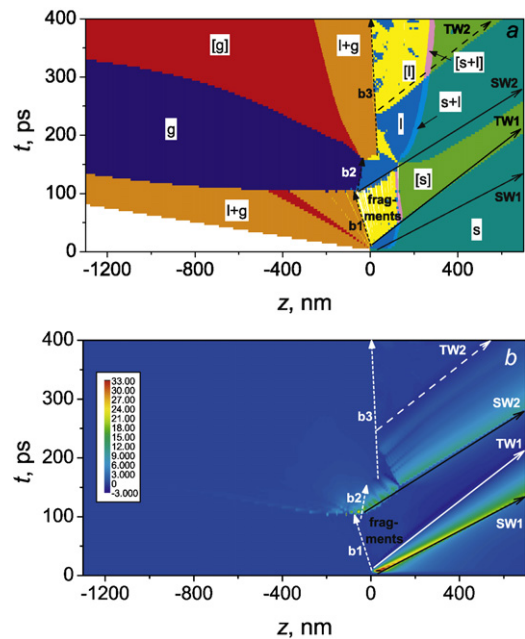


Fig. 4.  $z$ - $t$  diagrams of phase states (a) and pressure (b) in the target at  $\tau_{\text{delay}} = 100$  ps. Designations are the same as in Fig. 3.

plume tail. This, in turn, leads to the decrease of the crater depth (see Fig. 1).

To compare the results of modeling with experiment of Ref. [4] the crater depth  $\Delta$  for different delays has been estimated. To this end we integrate the mass flux through the plane  $z=0$  (initial surface position) by using the formula  $\Delta(t) = \rho_0^{-1} \int_0^t (\rho u)|_{z=0} dt'$ , where  $\rho_0$  is the initial material density and  $u$  is the material velocity. The dynamics of crater formation is presented elsewhere [6]; in this work in Fig. 1 the ultimate crater depth for  $t \rightarrow \infty$  (triangles) is presented. Already for the 10 ps delay the crater depth is similar to the one for a SP; for longer delays (50 and 100 ps) the crater depth was obtained to be smaller than that in the case of SP.

#### 4. Summary

We summarize here the basic stages of the DP ablation process. The first laser pulse creates the SW, which propagates into the target. Behind the SW a TW forms and propagates through the liquid layer resulting in the mechanical fragmentation and ablation of this layer. When  $\tau_{\text{delay}}$  is much shorter than  $\tau_{\text{ei}}$ , only one SW and one TW appear. In this case, the ablation crater is formed by both pulses simultaneously as in the case of a SP of the same energy. When the delay is on the order of the relaxation time, the second pulse creates the second SW thus reducing the intensity of the first TW and the depth of the ablation crater decreases. Finally, for delays longer than the electron–ion relaxation time the ablation crater is formed by the first pulse only, whereas the second pulse reheats and decelerates the ablated material; the crater depth in this case can be smaller than that for the SP.

#### Acknowledgments

The authors thank Dr. V.V. Milyavskiy for helpful discussions. This work was supported by the Centre National de la Recherche

Scientifique and the Russian Academy of Sciences (French-Russian collaboration project CNRS-ASRF 21276), the Russian Foundation for Basic Research (grants 08-08-01055 and 09-08-01129), and the Ministry of Education and Science of the Russian Federation (the Federal targeted program 'Scientific and scientific-pedagogical personnel of the innovative Russia' 2009–2013).

#### References

- [1] D.A. Cremers, L.J. Radziemski (Eds.), *Handbook of Laser-Induced Breakdown Spectroscopy*, Wiley, New York, 2006.
- [2] A. Semerok, C. Dutouquet, Ultrashort double pulse laser ablation of metals, *Thin Solid Films* 453–454 (2004) 501–505.
- [3] T. Donnelly, J.G. Lunney, S. Amoruso, R. Bruzzese, X. Wang, X. Ni, Double pulse ultrafast laser ablation of nickel in vacuum, *J. Appl. Phys.* 106 (2009) 013304.
- [4] S. Noël, J. Hermann, Reducing nanoparticles in metal ablation plumes produced by two delayed short laser pulses, *Appl. Phys. Lett.* 94 (2009) 053120.
- [5] D.R. Lide (Ed.), *CRC Handbook of Chemistry and Physics*, 87th ed., CRC Press, 2007, pp. 2006–2007.
- [6] M.E. Povarnitsyn, T.E. Itina, K.V. Khishchenko, P.R. Levashov, Suppression of ablation in femtosecond double-pulse experiment, *Phys. Rev. Lett.* 103 (2009) 195002.
- [7] M.E. Povarnitsyn, T.E. Itina, P.R. Levashov, K.V. Khishchenko, Multi-material two-temperature model for simulation of ultrashort laser ablation, *Appl. Surf. Sci.* 253 (2007) 6343–6346.
- [8] M.E. Povarnitsyn, T.E. Itina, M. Sentis, P.R. Levashov, K.V. Khishchenko, Material decomposition mechanisms in femtosecond laser interactions with metals, *Phys. Rev. B* 75 (2007) 235414.
- [9] M.E. Povarnitsyn, K.V. Khishchenko, P.R. Levashov, Phase transitions in femtosecond laser ablation, *Appl. Surf. Sci.* 255 (2009) 5120–5124.
- [10] L.D. Landau, E.M. Lifshits, *Statistical Physics*, Pergamon Press, Oxford, 1980.
- [11] N. Andreev, V. Fortov, E. Kazakov, K. Khishchenko, O. Kostenko, T. Kuehl, P. Levashov, M. Povarnitsyn, O. Rosmej, Y. Zhao, J. Duan, J. Liu, Interaction of phelix laser pulses with nanostructured targets: experiment and modeling, in: V.E. Fortov, et al. (Eds.), *Physics of Extreme States of Matter—2009*, IPCP, Chernogolovka, 2009, pp. 18–20.
- [12] E.D. Palik, *Handbook of Optical Constants of Solids*, Academic Press INC, 1985.
- [13] M. Veysman, B. Cros, N.E. Andreev, G. Maynard, Theory and simulation of short intense laser pulse propagation in capillary tubes with wall ablation, *Phys. Plasmas* 13 (2006) 053114.